

## Bone Tissue Formation under Ideal Conditions in a Scaffold Generated by a Reaction-Diffusion System

Marco A.Velasco\* and Diego A. Garzón-Alvarado†

**Abstract:** The design of porous scaffolds for tissue engineering requires methods to generate geometries in order to control the stiffness and the permeability of the implant among others characteristics. This article studied the potential of the reaction-diffusion systems to design porous scaffolds for bone regeneration. We simulate the degradation of the scaffold material and the formation of new bone tissue over canal-like, spherical and ellipsoid structures obtained by this approach. The simulations show that the degradation and growth rates are affected by the form of porous structures. The results have indicated that the proposed method has potential as a tool to generate scaffolds with internal porosities and is comparable with other methodologies to obtain this type of structures.

**Keywords:** bone scaffold; regeneration; reaction-diffusion; mathematical model.

### 1 Introduction

Scaffolds are fundamental tools for the regeneration of lost or damaged tissues and have become an important tool in tissue engineering [1]. Their functions, from the mechanical point of view, consist of bearing external loads and giving shape to the tissue that is regenerated on it [2-4]. From the biological point of view, those structures support the development of extracellular matrix and cell colonization. In addition, scaffolds should allow a sufficient transit of nutrient substances from the surrounding tissue or the culture media and waste disposal coming from the tissue being formed. Therefore, stiffness and mechanical resistance of the scaffold are the most important properties, from the mechanical standpoint and, from the point of view of substance transport, the most important is permeability.

---

\* Mechanical Engineering Applications and Research Group, Universidad Santo Tomás, Cra 9 No. 51-11, Bogotá, Colombia, marcovelasco@usantotomas.edu.co

† Research group on numerical methods for engineering (GNUM), Universidad Nacional de Colombia, Cra 30 No. 45-03, Bogotá, Colombia, dagarzona@unal.edu.co

An additional desirable feature of the scaffolds must be a controlled degradation after they are implanted in order to get void space where new tissue can grow. The mechanical properties and degradation of the scaffold depends on the material properties and the porosity geometry of its structure, meanwhile permeability depends on its structure. The mechanical properties of the scaffold must be similar to the properties of the replaced bone tissue in order to prevent stress shielding. Finally, the degradation rate must be as close as possible to the tissue growth rate to maintain stable properties in the compound tissue-scaffold during the regeneration process.

The development of scaffolds to promote cellular growth inside them has been one of the fundamental goals of bone tissue engineering [5–7]. The selection of a biocompatible, biodegradable material with certain mechanical properties is the first step for the design and production of the scaffold. Biocompatibility means that cells must adhere, proliferate, produce extracellular matrix and avoid a severe immune response. For example, inflammation should be avoided because it can decrease the regeneration rate and promote tissue rejection. Biodegradability is important because it is expected that, as long as cells proliferate, the void space in the scaffold increases and the degradation products of the scaffold material not to be toxic. Considering the foregoing, there are two different and complex processes: the degradation of the scaffold, which decreases its mechanical properties and regeneration, and the growth and maturation of tissue that increases stiffness and mechanical resistance of new bone. Therefore, experimental [8–16] and computational [3, 17–33] models are required to show the evolution of the system over time and to help to identify the optimal initial properties of the scaffold at the moment of the implant.

Computer simulations allow analyzing the scaffold properties and their effect on the rate of growth and mechanical behavior of the tissue. Those models vary as different properties, assumptions, domains and solving approaches are considered. From the geometric point of view the most studied property is the porosity [34–37]. It is especially important in those implants obtained by conventional methods such as particle leaching [16, 38], or electrospinning [39]. On the other hand, the development of rapid prototyping methods that allow greater control over the internal geometry of the scaffold has generated interest in the effect of the shape and size of the pores of the scaffold. In those studies, a representative volume element (RVE), instead of the whole model of the scaffold, is studied [3, 22]. Considering the size of the domain and phenomena that must be analyzed, simulations have been developed from different scales, from the microscopic to the macroscopic scale. At a nanoscale, the mechanisms of cell adhesion to the walls can be studied [40–42]. In the microscale, the effect of the shape and size of the pores can be

considered [3, 22], and, at the meso and macroscale, the external shape of the scaffold and the effect of mechanical loads acting on it [43–45]. Finally, the use of homogenization and multiscale methods has allowed the researching of various phenomena influencing the process of bone regeneration [46–50] like substances transport [51–54].

Several types of pore geometries have been proposed to analyze their effects on tissue growth. Scaffold designers have considered cubes, spheres and other geometries to analyze the effect of the pore shape in the regeneration process. It is found that spherical pores promote a more uniform growth of bone tissue [3, 22, 55]. There are more complex surfaces, such as gyroids [56, 57], which have the advantage of higher surface with respect to the volume in which they are contained. Also, topology optimization has been used [58–60] and reaction-diffusion patterns [61] that simulate processes occurring in the nature [62–65] to model the formation of pores. In this line of work, several authors have applied the reaction-diffusion systems in the process of calcium metabolism in vertebrates [66], the bone remodeling process [67] and the processes of bone morphogenesis [68, 69].

Although much work has been developed in both experimental and computational modeling, there are not final conclusions about the optimal internal geometry and material of a scaffold for bone regeneration. For example, the overall porosity range is quite wide, from 50 to 90% for scaffolds that are not subjected to mechanical loads [70]. The recommended size of the pores varies between 150 and 600  $\mu\text{m}$  [71] and from 400 to 1200  $\mu\text{m}$  [72]. The variety of conclusions may be due to, as stated by Bohner et al [73], the problem of optimizing the function of a scaffold is multivaried and multiobjective. Under this consideration, this article proposes an ideal bone formation and the degradation of a scaffold with internal geometry obtained from a reaction-diffusion system. The advantage of an architecture generated by a reaction-diffusion system for a porous scaffold lies in the hypothesis of the self-assembly of its structure. This allows obtaining a desired pore distribution with an adequate control of the variables of the chemical process. For this purpose, we have modeled the formation of the scaffold by reaction-diffusion equations of the type Schnakenberg [74] with parameters in the space of Turing [61]. This type of equations allows choosing the parameters according to the size and distribution of the pores. On the other hand, to model the degradation, we have used the model proposed by Adachi et al [3]. Finally, bone growth takes place, hypothetically, in those void spaces that appear where the scaffold degrades. The results indicated that the proposed method has a good potential to obtain a new generation of scaffold geometries.

## 2 Materials and Methods

We assume a model consisting of three processes as showed in figure 1.

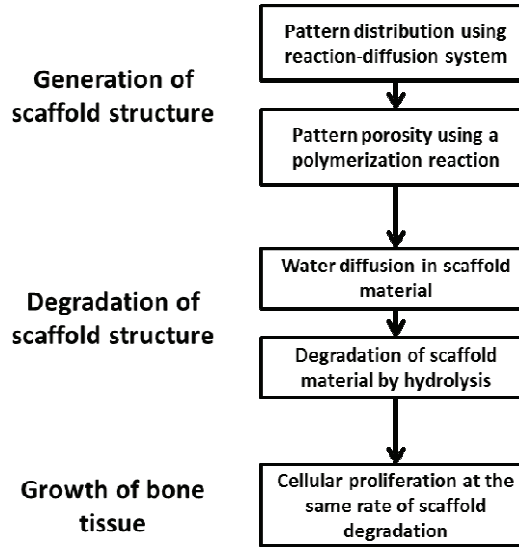


Figure 1: Stages of generation and degradation of the scaffold using reaction-diffusion processes

### 2.1 Generation of a scaffold structure

The geometry of a representative volume element of a scaffold can be obtained by the model proposed by Garzón-Alvarado et al [61]. In that article, the distribution and size of the pores is obtained by a reaction-diffusion system besides a polymerization reaction. To this purpose, a Schnakenberg reaction-diffusion system is considered, in which the reaction rate is directly proportional to the product of the active concentrations of the reactants. Thus, the reaction kinetics is described by Eq. 1:

$$\begin{aligned} \frac{\partial[X]}{\partial t} &= D_1\Delta[X] + K_1[A] - K_2[X] + K_3[X]^2[Y] \\ \frac{\partial[Y]}{\partial t} &= D_2\Delta[Y] + K_4[B] - K_3[X]^2[Y] \end{aligned} \quad (1)$$

Where X and Y are two hypothetical reactants that form the required structure of the scaffold. Equation (1) only depends on the variables X and Y because the values  $D_1, D_2, A, B, K_1, K_2, K_3$  and  $K_4$  are positive constants. Here, we use the

methodology suggested by Garzón-Alvarado et al [61] in order to obtain a dimensionless model of the reaction-diffusion. The dimensionless equation is:

$$\begin{aligned} \frac{\partial u}{\partial t} - \nabla^2 u &= \gamma(a - u + u^2 v) \\ \frac{\partial v}{\partial t} - d \nabla^2 v &= \gamma(b - u^2 v) \end{aligned} \quad (2)$$

where  $a, b, u$  and  $v$  are the dimensionless forms of  $A, B, X$  and  $Y$  variables,  $\gamma$  and  $d$  are dimensionless constants. Here,  $u$  and  $v$  are the concentration of reactants in the considered domain and  $d$  is the diffusion constant. After this, we apply an analysis of Turing instabilities in order to obtain different combinations of variables values, generating patterns described by wave numbers. A detailed explanation of this process is provided in Leppänen et al. [75].

Once the desired pattern is obtained for the reaction-diffusion system, it is assumed that there must be a biopolymer that copies the pattern of  $X$  or  $Y$  and develops the scaffold. To model this process, it is supposed that the polymerization follows a law similar to the one presented in Murray [76]. This process is described below:

$$\frac{dM}{dt} = C \frac{[X]^r}{[X]^r + [S]^r} \frac{t^p}{t^p + T^p} \quad (3)$$

Where  $S$  is the threshold value of the concentration of the reagent  $X$  that initiates polymerization,  $M$  is the concentration of biomaterial,  $t$  is the time from the start of the polymerization process,  $T$  is the threshold value of time when the polymerization begins,  $C$  is the constant rate of polymerization, and  $p$  and  $r$  are constants defining the slope of the threshold function (see [61]).

## **2.2 Degradation Model of the Scaffold**

For the degradation model, we assume that the biopolymer degrades by hydrolysis in a similar manner as the polylactic acid (PLA) or others polyesters. This study adopts the degradation model of Adachi et al (3). In that model the elastic modulus  $E_s$  is proportional to the molecular weight of the polymer:

$$E_s(W(t)) = E_{s0} \frac{W(t)}{W_0} \quad (4)$$

where  $E_{s0}$  is the elasticity modulus corresponding to an initial molecular weight  $W_0$ .

In turn, as water diffuses into the polymer and brakes molecular bonds, the molecular weight of the polymer decreases over time as described in Eq. 5:

$$W(c) = -\beta c \quad (5)$$

Where  $\beta$  is a biomaterial constant that describes the velocity at which it degrades and  $c$  is the concentration value of water. This  $c$  value changes over time according to the diffusion process described in Eq. 6:

$$\dot{c} = \alpha \nabla^2 c \quad (6)$$

where  $\alpha$  is the diffusion coefficient of water in the biopolymer.

The properties of the material considered above are taken from Adachi et al [3] and are similar to polylactic acid properties with an elasticity modulus of  $E_{s0}=20\text{GPa}$ , initial molecular weight  $W_0=70000\text{g/mol}$ , diffusion coefficient  $\alpha = 4.0 \times 10^{-4}\text{mm}^2/\text{day}$  and degradation rate constant  $\beta = 4000/\text{day}$ .

### 2.3 Bone Formation Model

Moreover, as the scaffold degrades, we assume an ideal process where immature bone tissue is generated without the need of a mechanical load stimulus. So, the new tissue fills the space left by the scaffold material that has been degraded.

### 2.4 Computational Implementation

The model of reaction-diffusion, degradation and tissue growth was implemented using the finite element method applied to a cubic mesh of 17576 node and 15625 elements. The side of the cube is assumed to be 2.4 mm. All simulations employ a step increment of  $\Delta t= 1$  day, until it reaches 100 days. The selection of the initial conditions is random and it was considered that at the boundaries of the domain the flow is null.

## 3 Results

This section presents the results of the degradation of the scaffold and the growth of bone tissue on it. Numerical tests were carried out with different parameters of the reaction-diffusion system in order to obtain three wave numbers that result into different geometrical configurations. Thus, the structure obtained from a wave number (2,2,0) determines an inner structure formed by canals of uniform thickness, the structure obtained with the wave number (2,2,2) represents relatively uniform pores similar to a sphere and the wave number (4,2,2) would result into pores similar to ellipsoids.

### 3.1 Scaffold canal-shaped

Figure 2 shows the formation of the microstructure obtained for the variables  $u$  and  $v$ , when  $s$  is equal to 0,995 using the wave number (2,2,0). The RD system

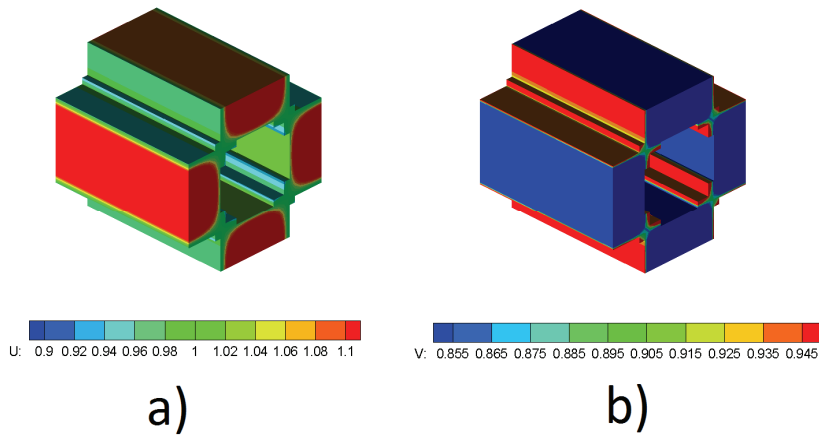


Figure 2: Representative volume element obtained with a wave number  $(2,0,0)$ . a) Concentration value for the variable  $u$ . b) Concentration value for the variable  $v$ .

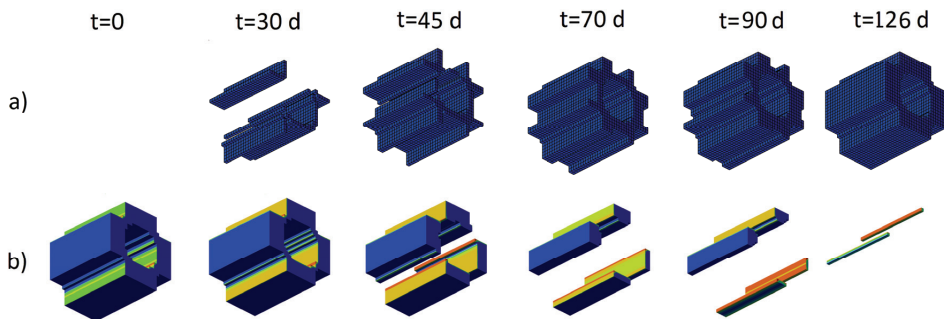


Figure 3: Bone tissue regeneration and scaffold degradation in a representative volume element obtained with a wave number  $(2,0,0)$ . a) Growth of bone tissue. b) Degradation of the scaffold.

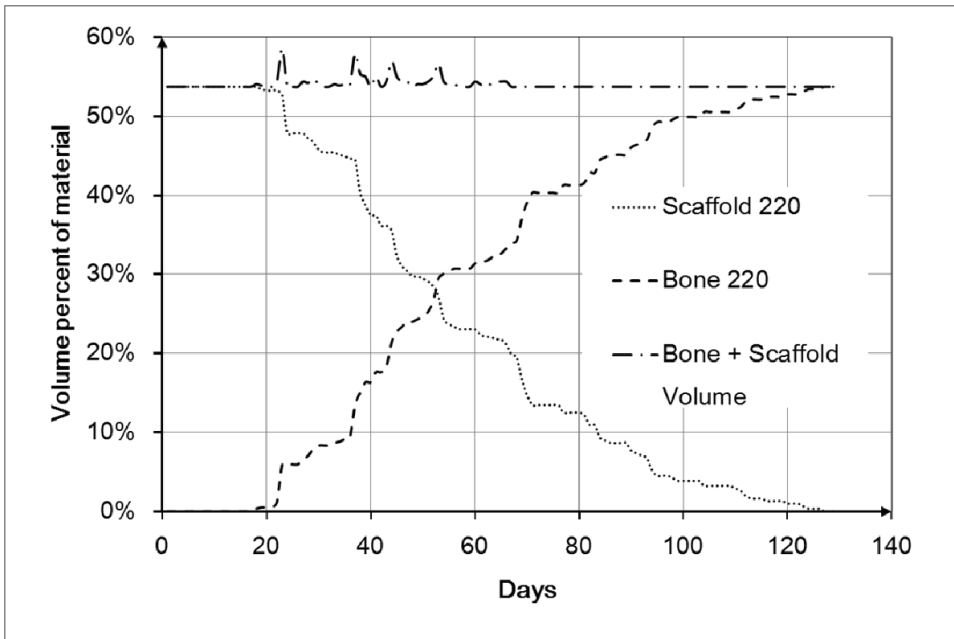


Figure 4: Bone tissue regeneration and scaffold degradation in a representative volume element obtained with a wave number (2,0,0) as a function of time.

parameters were  $d= 8.6676$ ,  $a= 0.1$ ,  $b= 0.9$  and  $\gamma= 230.82$ . The Turing pattern stabilized at a dimensionless time of  $t = 5.8$ , with a resulting porosity of 46%. The trabecular width obtained from the unit cell is 1.2 mm. Figures 3 (a) and 3 (b) show the tissue regeneration and scaffold degradation, respectively. Figure 4 shows the percentage of remaining volume of the scaffold as a function of time expressed in days. It is observed that 127 days are required for degradation and complete regeneration.

### 3.2 Scaffold with spherical pores

Figure 5 shows the formation of the microstructure obtained for the variables  $u$  and  $v$ , when  $s$  is equal to 0,895 using the wave number (2,2,2). The RD system parameters were  $d= 8.6123$ ,  $a= 0.1$ ,  $b= 0.9$  and  $\gamma= 346.3578$ . The Turing pattern stabilized at a dimensionless time of  $t = 8.4$ , with a resulting porosity of 32%. The trabecular width obtained from the unit cell is 1.2 mm. Figures 6 (a) and 6 (b) show the tissue regeneration and scaffold degradation, respectively. Figure 7 shows the percentage of remaining volume of the scaffold as a function of time expressed in days. It is observed that 118 days are required for degradation and complete

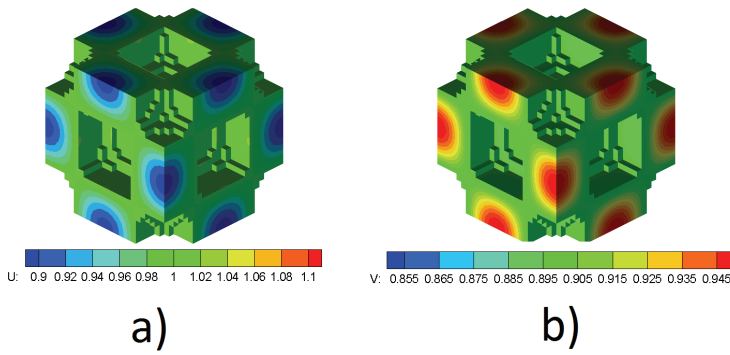


Figure 5: Representative volume element obtained with a wave number (2,2,2). a) Concentration value for the variable  $u$ . b) Concentration value for the variable  $v$ .

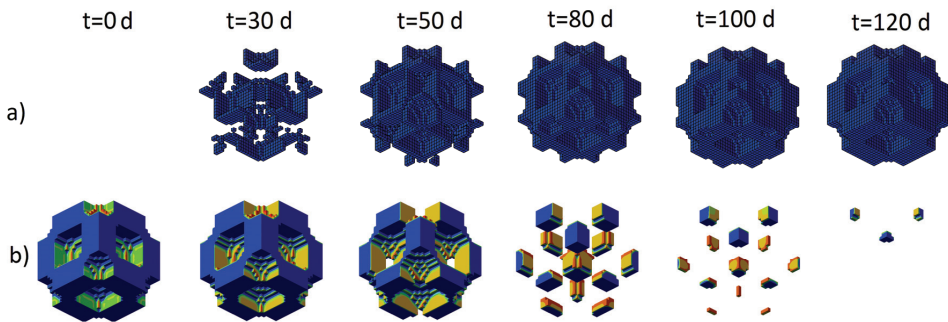


Figure 6: Bone tissue regeneration and scaffold degradation in a representative volume element obtained with a wave number (2,2,2). a) Growth of bone tissue. b) Degradation of the scaffold.

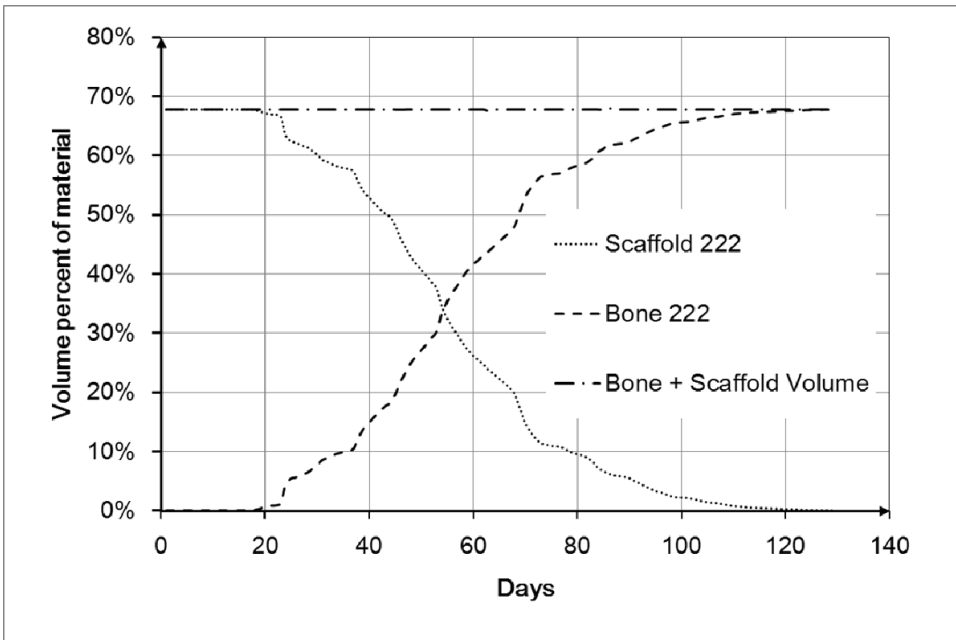


Figure 7: Bone tissue regeneration and scaffold degradation in a representative volume element obtained with a wave number (2,2,2) as a function of time.

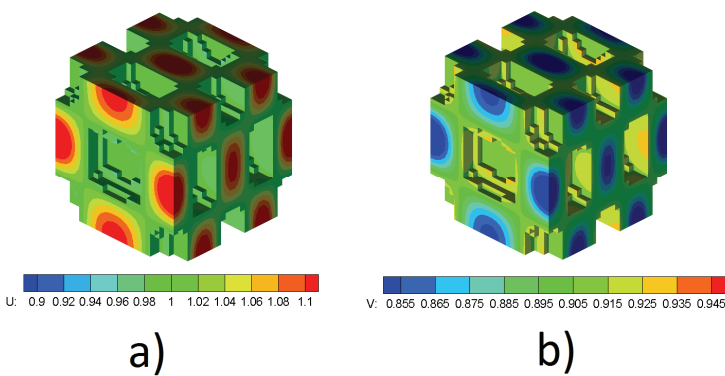


Figure 8: Representative volume element obtained with a wave number (4,2,2). a) Concentration value for the variable  $u$ . b) Concentration value for the variable  $v$ .

regeneration.

### 3.3 Scaffold with ellipsoid pore

Figure 8 shows the formation of the microstructure obtained for the variables  $u$  and  $v$ , when  $s = 0.995$  using the wave number (4,2,2). The RD system parameters are  $d = 8.5736$ ,  $a = 0.1$ ,  $\gamma = 700.4675$ ,  $b = 0.9$ . The Turing pattern stabilized at a dimensionless time of  $t = 28.8$ , with a resulting porosity of 29.6%. The trabecular width obtained from the unit cell is 0,6 mm. Figures 9 (a) and 9 (b) show the tissue regeneration and scaffold degradation, respectively. Figure 10 shows that for this configuration, 91 days are required for the scaffold degradation and tissue regeneration.

Finally, figure 11 shows the evolution of the normalized mass remaining as a function of time as the degradation process occurs. After 20 days, the degradation begins to be considerable. It can be observed that the use of reaction-diffusion systems with high wave number and higher porosity (4,2,2) decreases the time necessary for a complete degradation. We can also see that the degradation process in highly porous structures with wave number (4,2,2), have higher smoothness in the evolution of degradation process and bone formation than in structures with wave number (2,2,0).

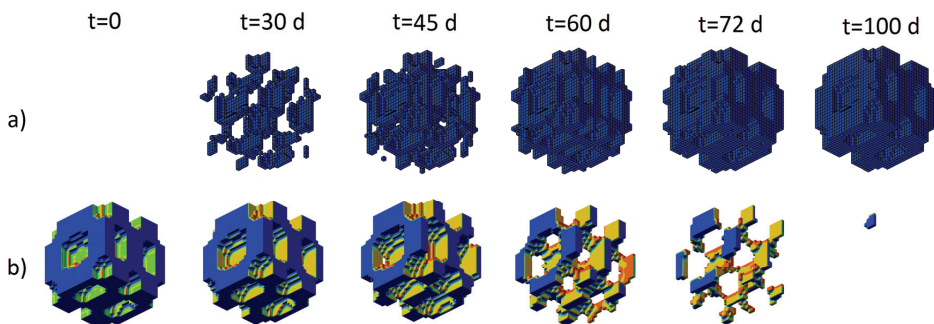


Figure 9: Bone tissue regeneration and scaffold degradation in a representative volume element obtained with a wave number (4,2,2). a) Growth of bone tissue. b) Degradation of the scaffold.

## 4 Discussion

This article has shown the use of a hypothetical model consisting of a reaction-diffusion system and a polymerization reaction. This system allows generating

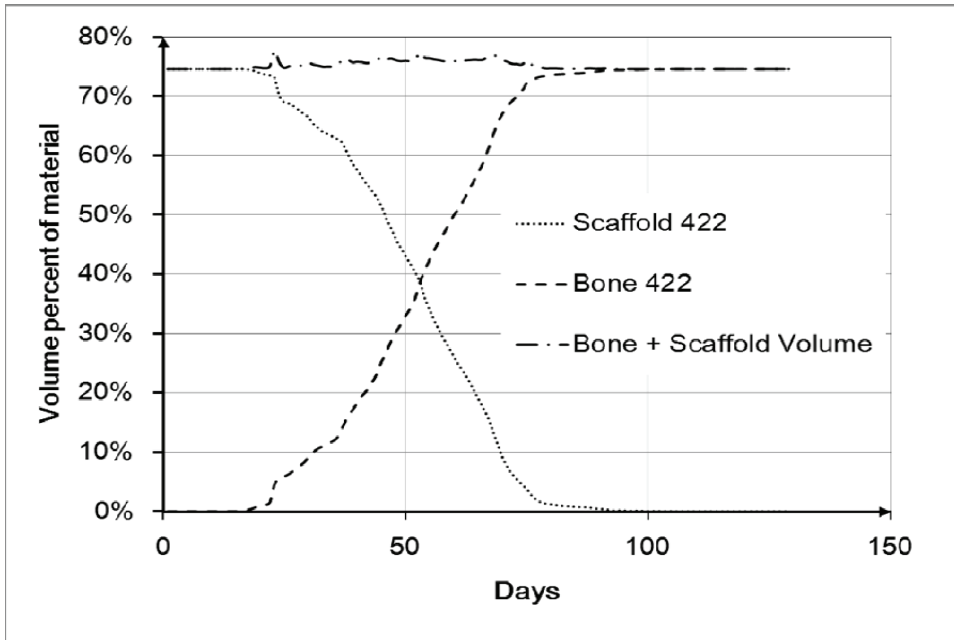


Figure 10: Bone tissue regeneration and scaffold degradation in a representative volume element obtained with a wave number (4,2,2) as a function of time.

geometries that may be used in the design of porous scaffolds geometries for applications in bone tissue engineering. Three spatial distributions of pores were obtained by varying the parameters  $a$ ,  $b$ ,  $d$ ,  $\gamma$ ,  $T_a$ , of a reaction-diffusion system of Schnakenberg [61]. The obtained wave number  $w$  determines the frequency of the spatial distribution of the pores as seen in Figures 2, 5 and 8. The decrease of value  $d$  and the increase of the value  $\gamma$  led to the formation of the patterns that have a higher wave number. The wave number (2,2,0) is obtained with  $d = 8.6676$  and  $\gamma = 230.82$  and the wave number (4,2,2) is obtained with  $d = 8.6123$  and  $\gamma = 346.36$ . The nonlinear behavior of the reaction-diffusion system is observed when small changes of the value  $d$  cause significant changes in the wave number of the obtained pattern. We can also observe in Figures 2, 5 and 8 that pores with greater sphericity and higher rates of degradation can be obtained by increasing the value of the wave numbers. It is noteworthy that the degradation rates have a more stable and smoother behavior in time as the wave number increases and the degradation time becomes smaller as shown in Figure 11. Furthermore, the total porosity of the element that depends on the size of the pores was changed varying the threshold value  $s$  used in the polymerization reaction.

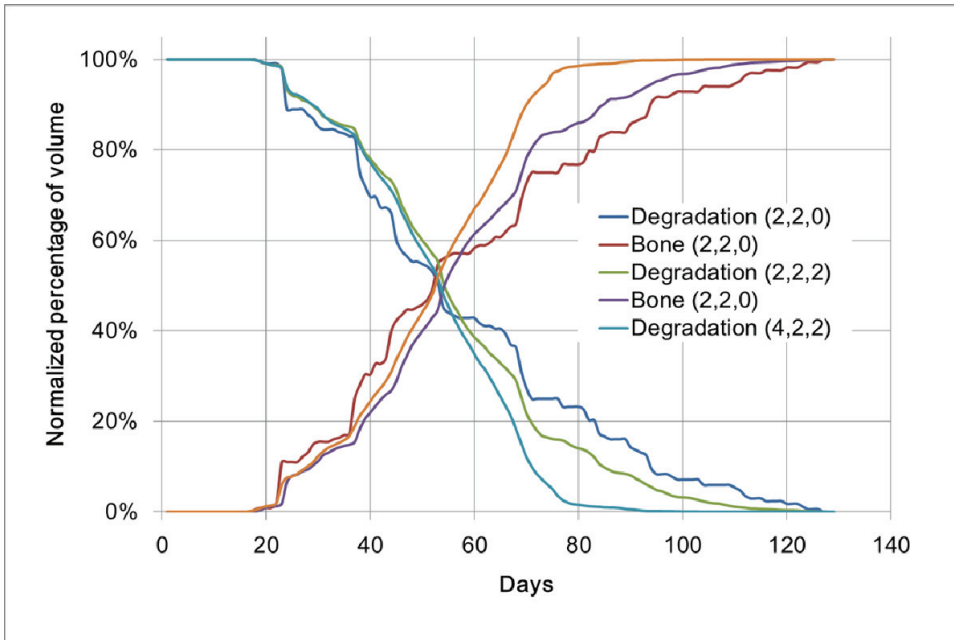


Figure 11: Standard masses remaining in the degradation time of the three volumes considered for different wave numbers.

As we can see in Figure 11, the simulations do not show an appreciable degradation in the first 20 days. This may be due to the time required to increase the concentration value of water in the interior of the trabeculae of the scaffold to be high enough to break the sufficient amount of molecular bonds. This allows the degradation of scaffold solid portion. From day 20 until day 50, approximately, we observed similar degradation rates (see Figure 11). Finally, from day 50 there is degradation at different rates that lead to a high decrease of the mass in the element with ellipsoids pores.

Comparing with previous work, we can see that different approaches lead to similarities in the internal architecture of the scaffold. For example, from considerations of topology optimization, Almeida et al. [60] obtained structures similar to the canals and ellipsoids reported in this article. It is also noteworthy that the structures obtained in this work are similar to the surfaces used in previous works with gyroids surfaces [56, 57]. There is a previous report where reaction-diffusion systems may cause this type of surfaces [77]. On the other hand, the implementation of the model has a low computational cost since it required about 1000 or less time steps to model the complete degradation of each of the elements of the scaffold.

## 5 Conclusion

This work has made some simplifications that must be detailed. In the model for the generation of the structure, there is simplification of the domain size and consideration of null flow in the reaction-diffusion system boundaries. Furthermore, in the degradation model, we considered that the size of the walls or trabeculae obtained is slim enough to adopt a degradation model that does not take into account the effects of autocatalytic inherent to hydrolysis of PLA as stated by Chen [22]. However, this work provides a possible line of research in tissue engineering by proposing another way to get internal geometries for scaffolds from reaction-diffusion systems. An extension of this study is necessary in order to analyze the effect of domain size and elements of the mesh used in the FEM method with respect to the wavelength of the patterns obtained. It is also convenient to carry out an analysis of the mechanical behavior of the system scaffold degradation - tissue regeneration when is subjected to loads such as pressures on different sides of the representative volume elements.

### Competing interests

The authors declare that they have no competing interests.

### Authors' contributions

The work was made by equal parts, in manuscript, modeling and numerical simulation. All authors read and approved the final manuscript.

**Acknowledgement:** This work was financially supported by the Bogotá Research Division of Universidad Nacional de Colombia, under the modality: “Strengthening of research and artistic creation groups with national projection. Groups Alliances”. The Project title is “Programa para la obtención y validación de parámetros numéricos utilizados en modelos matemáticos y simulación de sistemas y procesos biológicos mediante el diseño y caracterización de modelos celulares in vitro”, Hermes code 12873, and the Research Unit of Universidad Santo Tomás, under the modality: “Fodein Call”, internal code 6013011102.

## References

1. Ikada Y (2006) Challenges in tissue engineering. *Interface* 3:589–601.
2. Chen Y, Zhou S, Li Q (2011) Microstructure design of biodegradable scaffold and its effect on tissue regeneration. *Biomaterials* 32:5003–14.
3. Adachi T, Osako Y, Tanaka M, Hojo M, Hollister SJ (2006) Framework for optimal design of porous scaffold microstructure by computational simula-

- tion of bone regeneration. *Biomaterials* 27:3964–3972.
4. Hollister SJ, Maddox RD, Taboas JM (2002) Optimal design and fabrication of scaffolds to mimic tissue properties and satisfy biological constraints. *Biomaterials* 23:4095–103.
  5. Hollister SJ (2005) Porous scaffold design for tissue engineering. *Nat. Mater.* 4:518–524.
  6. Hutmacher DW (2000) Scaffolds in tissue engineering bone and cartilage. *Biomaterials* 21:2529–43.
  7. Schieker M, Seitz H, Drosse I, Seitz S, Mutschler W (2006) Biomaterials as Scaffold for Bone Tissue Engineering. *Eur J Trauma* 32:114–124.
  8. Cao Y et al. (2006) The influence of architecture on degradation and tissue ingrowth into three-dimensional poly (lactic-co-glycolic acid) scaffolds in vitro and in vivo. *Biomaterials* 27:2854–2864.
  9. Laschke MW, Strohe A, Scheuer C, Eglin D, Verrier S (2009) In vivo biocompatibility and vascularization of biodegradable porous polyurethane scaffolds for tissue engineering. *Acta Biomater.* 5:1991–2001.
  10. Deschamps AA et al. (2004) In vivo and in vitro degradation of poly(ether ester) block copolymers based on poly(ethylene glycol) and poly(butylene terephthalate). *Biomaterials* 25:247–258.
  11. Tsuji H, Ikarashi K (2004) In vitro hydrolysis of poly(L-lactide) crystalline residues as extended-chain crystallites. Part I: long-term hydrolysis in phosphate-buffered solution at 37 degrees C. *Biomaterials* 25:5449–55.
  12. Kirkpatrick CJ et al. (2005) In vitro methodologies to evaluate biocompatibility: status quo and perspective. *ITBM-RBM* 26:192–199.
  13. Vailhé B, Vittet D, Feige JJ (2001) In vitro models of vasculogenesis and angiogenesis. *Lab Invest.* 81:439–452.
  14. Kim H, Camata RP, Chowdhury S, Vohra YK (2010) In vitro dissolution and mechanical behavior of c-axis preferentially oriented hydroxyapatite thin films fabricated by pulsed laser deposition. *Acta Biomater.* 6:3234–3241.
  15. Buma P, Schreurs W, Verdonchot N (2004) Skeletal tissue engineering - from in vitro studies to large animal models. *Biomaterials* 25:1487–1495.

16. Kang Y et al. (2009) A study on the in vitro degradation properties of poly(L-lactic acid)/beta-tricalcium phosphate (PLLA/beta-TCP) scaffold under dynamic loading. *J. Biomed. Eng.* 31:589–594.
17. Chung CA, Lin TH, Chen SD, Huang HI (2010) Hybrid cellular automaton modeling of nutrient modulated cell growth in tissue engineering constructs. *J. Theor. Biol.* 262:267–278.
18. Schantz JT, Brandwood A, Hutmacher DW, Khor HL, Bittner K (2005) Osteogenic differentiation of mesenchymal progenitor cells in computer designed fibrin-polymer-ceramic scaffolds manufactured by fused deposition modeling. *J Mater Sci Mater Med.* 16:807–19.
19. Voronov R, Van Gordon S, Sikavitsas VI, Papavassiliou D V (2010) Computational modeling of flow-induced shear stresses within 3D salt-leached porous scaffolds imaged via micro-CT. *J Biomech.* 43:1279–1286.
20. Pierre J et al. (2006) Modeling of large bone implant culture in a perfusion bioreactor. *J Biomech.*39:S220 – S220.
21. Miranda P, Pajares A, Guiberteau F (2008) Finite element modeling as a tool for predicting the fracture behavior of robocast scaffolds. *Acta Biomater.* 4:1715–1724.
22. Chen Y, Zhou S, Li Q (2011) Mathematical modeling of degradation for bulk-erosive polymers: Applications in tissue engineering scaffolds and drug delivery systems. *Acta Biomater.* 7:1140–1149.
23. Komarova S V (2006) Bone remodeling in health and disease: lessons from mathematical modeling. *Ann. N. Y. Acad. Sci.* 1068:557–9.
24. Chung CA, Lin T-H, Chen S-D, Huang H-I (2010) Hybrid cellular automaton modeling of nutrient modulated cell growth in tissue engineering constructs. *J. Theor. Biol.* 262:267–278.
25. Hu Z et al. (2009) On Modeling Bio-Scaffolds: Structural and Fluid Transport Characterization Based on 3-D Imaging Data. *Tsinghua Sci. Technol.* 14:20–23.
26. Sanz-Herrera JA, Reina-Romo E (2011) Cell-biomaterial mechanical interaction in the framework of tissue engineering: insights, computational modeling and perspectives. *Int. J. Mol. Sci.* 12:8217–44.

27. Ochoa I et al. (2009) Permeability evaluation of 45S5 Bioglass -based scaffolds for bone tissue engineering. *Biomechanics* 42:257–260.
28. Sanz-Herrera JA, García-Aznar JM, Doblaré M (2009) On scaffold designing for bone regeneration: A computational multiscale approach. *Acta Biomater.*5:219–229.
29. Kang H, Lin C-Y, Hollister SJ (2010) Topology optimization of three dimensional tissue engineering scaffold architectures for prescribed bulk modulus and diffusivity. *Struct Multidiscip Optim.*42:633–644.
30. Hollister SJ, Lin CY (2007) Computational design of tissue engineering scaffolds. *Tissue Eng.* 196:2991–2998.
31. Lacroix D, Planell JA, Prendergast PJ (2009) Computer-aided design and finite-element modelling of biomaterial scaffolds for bone tissue engineering. *Philos Transact A Math Phys Eng Sci.* 367:1993–2009.
32. Sanz-Herrera JA, García-Aznar JM, Doblaré M (2009) A mathematical approach to bone tissue engineering. *Philos Transact A Math Phys Eng Sci.* 367:2055–2078.
33. Shipley RJ et al. (2009) Design criteria for a printed tissue engineering construct: a mathematical homogenization approach. *J. Theor. Biol.* 259:489–502.
34. Byrne DP, Prendergast PJ, Kelly DJ (2006) Optimisation of scaffold porosity using a stochastic model for cell proliferation and migration in mechanobiological simulations. *J Biomech.* 39:S413–S414.
35. Swider P et al. (2007) Use of high-resolution MRI for investigation of fluid flow and global permeability in a material with interconnected porosity. *J Biomech.* 40:2112–2118.
36. Singh R et al. (2010) Characterization of the deformation behavior of intermediate porosity interconnected Ti foams using micro-computed tomography and direct finite element modeling. *Acta Biomater.*6:2342–2351.
37. Byrne DP, Lacroix D, Planell JA, Kelly DJ, Prendergast PJ (2007) Simulation of tissue differentiation in a scaffold as a function of porosity , Young's modulus and dissolution rate: Application of mechanobiological models in tissue engineering. *Biomaterials.* 28:5544–5554.

38. Puppi D, Chiellini F, Piras a. M, Chiellini E (2010) Polymeric materials for bone and cartilage repair. *Prog Polym Sci.* 35:403–440.
39. Lim LT, Auras R, Rubino M (2008) Processing technologies for poly(lactic acid). *Prog Polym Sci.* 33:820–852.
40. Comisar WA, Kazmers NH, Mooney DJ, Linderman JJ (2007) Engineering RGD nanopatterned hydrogels to control preosteoblast behavior: A combined computational and experimental approach. *Biomaterials* 28:4409–4417.
41. Zhang S, Marini DM, Hwang W, Santoso S (2002) Design of nanostructured biological materials through self-assembly of peptides and proteins. *Curr Opin. Chem. Biol.* 6:865–871.
42. Chen VJ, Smith L a, Ma PX (2006) Bone regeneration on computer-designed nano-fibrous scaffolds. *Biomaterials* 27:3973–9.
43. Voronov R, VanGordon S, Sikavitsas VI, Papavassiliou D V (2010) Computational modeling of flow-induced shear stresses within 3D salt-leached porous scaffolds imaged via micro-CT. *J Biomech.* 43:1279–1286.
44. Sun W, Starly B, Nam J, Darling A (2005) Bio-CAD modeling and its applications in computer-aided tissue engineering. *Comput. Aided Des.* 37:1097–1114.
45. Karunratanakul K, Schrooten J, Oosterwyck H Van (2010) Finite element modelling of a unilateral fixator for bone reconstruction: Importance of contact settings. *Med Eng Phys.* 32:461–467.
46. Chaturvedi R et al. (2005) On multiscale approaches to three-dimensional modelling of morphogenesis. *J R Soc Interface.* 2:237–253.
47. Sanz-Herrera J, García-Aznar J, Doblaré M (2008) Micro-macro numerical modelling of bone regeneration in tissue engineering. *Comput Meth Appl Mech Eng.* 197:3092–3107.
48. Chan KS, Liang W, Francis WL, Nicolella DP (2010) A multiscale modeling approach to scaffold design and property prediction. *J. Mech. Behav. Biomed. Mater.* 3:584–93.
49. Shipley RJ et al. (2009) Design criteria for a printed tissue engineering construct: A mathematical homogenization approach. *J. Theor. Biol.* 259:489–502.

50. Miara B, Rohan E, Zidi M, Labat B (2005) Piezomaterials for bone regeneration design–homogenization approach. *J. Mech. Phys. Solids.* 53:2529–2556.
51. Sengers BG, Taylor M, Please CP, Oreffo ROC (2007) Computational modelling of cell spreading and tissue regeneration in porous scaffolds. *Biomaterials* 28:1926–40.
52. Ye H, Das DB, Triffitt JT, Cui Z (2006) Modelling nutrient transport in hollow fibre membrane bioreactors for growing three-dimensional bone tissue. *J. Membr. Sci.* 272:169–178.
53. Chung CA, Lin T, Chen S (2009) Hybrid cellular automaton modeling of nutrient modulated cell growth in tissue engineering constructs. *J. Theor. Biol.* 262:267–278
54. Karande TS, Ong JL, Agrawal CM (2004) Diffusion in musculoskeletal tissue engineering scaffolds: design issues related to porosity, permeability, architecture, and nutrient mixing. *Ann Biomed Eng.* 32:1728–43.
55. Chua CK, Leong KF, Cheah CM, Chua SW (2003) Development of a Tissue Engineering Scaffold Structure Library for Rapid Prototyping . Part 1: Investigation and Classification. *Tissue Eng.* 21:291–301.
56. Kapfer SC, Hyde ST, Mecke K, Arns CH, Schröder-Turk GE (2011) Minimal surface scaffold designs for tissue engineering. *Biomaterials* 32:6875–82.
57. Yoo DJ (2011) Porous scaffold design using the distance field and triply periodic minimal surface models. *Biomaterials* 32:7741–54.
58. Yu C, Kikuchi N, Hollister SJ (2004) A novel method for biomaterial scaffold internal architecture design to match bone elastic properties with desired porosity. *J Biomech.* 37:623–636.
59. Sturm S, Zhou S, Mai Y-W, Li Q (2010) On stiffness of scaffolds for bone tissue engineering—a numerical study. *J Biomech.* 43:1738–1744.
60. De Amorim Almeida H, Da Silva Bártolo PJ (2010) Virtual topological optimisation of scaffolds for rapid prototyping. *J. Biomed. Eng.* 32:775–782.
61. Garzón-Alvarado DA, Velasco MA, Narváez-Tovar CA (2011) Self-assembled scaffolds using reaction–diffusion systems: a hypothesis for bone regeneration. *J. Mech. Med. Biol.* 11:231–272.

62. Ristori S et al. (2007) Interplay between the Belousov-Zhabotinsky reaction-diffusion system and biomimetic matrices. *Chem. Phys. Lett.* 436:175–178.
63. Volpert V, Petrovskii S (2009) Reaction-diffusion waves in biology. *Phys. Life Rev.* 6:267–310.
64. Kondo S (2002) The reaction-diffusion system: a mechanism for autonomous-pattern formation in the animal skin. *Genes Cells.* 7:535–541.
65. Crampin EJ, Maini PK (2001) Reaction-diffusion models for biological pattern formation. *Methods Appl. Anal.* 8(3):415–428.
66. Courtin B, Perault-Staub AM, Staub JF (1995) Spatio-temporal self-organization of bone mineral metabolism and trabecular structure of primary bone. *Acta Biotheor.* 43:373–386.
67. Tezuka K, Wada Y, Takahashi A, Kikuchi M (2005) Computer-simulated bone architecture in a simple bone-remodeling model based on a reaction-diffusion system. *J. Bone Miner. Res.* 23:1–7.
68. Garzón-Alvarado DA, García-Aznar JM, Doblaré M (2009) A reaction-diffusion model for long bones growth. *Biomech. Model. Mechanobiol.* 8:381–395.
69. Garzón-Alvarado DA, García-Aznar JM, Doblaré M (2009) Appearance and location of secondary ossification centres may be explained by a reaction-diffusion mechanism. *Comput. Biol. Med.* 39:554–561.
70. K. Whang, K.E. Healy, D.R. Elenz, E.K. Nam, D.C. Tsai, C.H. Thomas, G.W. Nuber, F.H. Glorieux, R. Travers and SMS (1999) Engineering Bone Regeneration with Bioabsorbable Scaffolds with Novel Microarchitecture. *Tissue Eng.* 5:35–51.
71. Cornell CN (1999) Osteoconductive materials and their role as substitutes for autogenous bone grafts. *Orthop Clin North Am.*30:591–598.
72. Hollister SJ et al. (2005) Engineering craniofacial scaffolds. *Orthod Craniofac Res.* 8:162–73.
73. Bohner M, Loosli Y, Baroud G, Lacroix D (2011) Commentary: Deciphering the link between architecture and biological response of a bone graft substitute. *Acta Biomater.* 7:478–484.
74. Maini PK (1997) Spatial pattern formation in chemical and biological systems. *J. Chem. Soc., Faraday Trans.* 93:3601–3610.

75. Leppänen T, Karttunen M, Barrio R, Kaski K (2003) Turing systems as models of complex pattern formation. *Braz J Phys.*34:368–372.
76. Murray JD (1993) *Mathematical Biology II: Spatial models and biomedical applications* (Springer-Verlag).
77. Shoji H, Yamada K, Ueyama D (2007) Turing patterns in three dimensions. *Phys Rev E.* 75:1–13.

